

Active control of gear mesh vibration using a permanent-magnet synchronous motor and simultaneous equation method

Dominik Reitmeier, M.Sc.

Leibniz University Hannover - Institute for Drive Systems and Power Electronics

Welfengarten 1

30167 Hannover, Germany

Phone: +49 (0)511 762 4231

Fax: +49 (0)511 762 3040

Email: dominik.reitmeier@ial.uni-hannover.de

URL: <https://www.ial.uni-hannover.de>

Keywords

«Acoustic noise», «Active damping», «Adaptive control», «Mechatronics», «Control of drive»

Abstract

This paper presents an active vibration control (AVC) for gear mesh vibrations. The vibrations are reduced by an additional motor torque. To determine the amplitude and phase of the torque without prior identification of the controlled system parameters, a narrowband AVC using the simultaneous equation method is presented.

Introduction

Many drivetrains use gearboxes or transmissions to convert speed and torque from one rotating power source to another. During power transmission, internal excitation mechanisms generate periodic vibrations. These vibrations propagate through the shafts and bearings to the housing, where they are emitted as an acoustic noise. The spectrum of the noise contains individual multiples of the speed and is audible as a whining sound. Gear whine is a problem particularly in electric vehicles, since the combustion engine no longer masks this noise. This vibration and monotonous noise can also be disturbing in other applications.

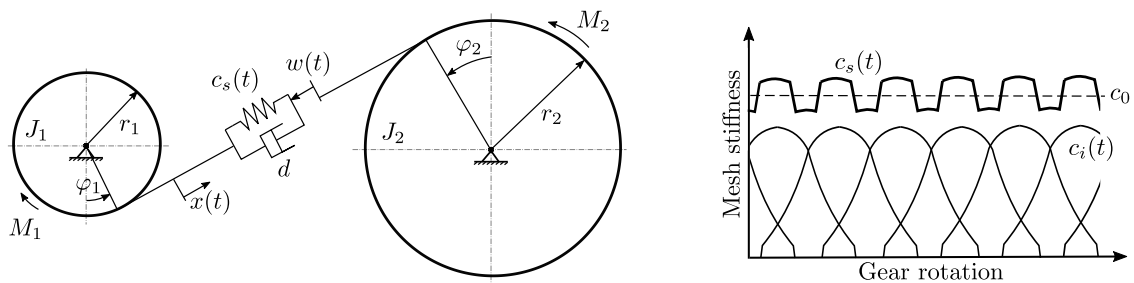


Fig. 1: Dynamic model of a one stage gear system [1]

Several sources contribute to the generation of noise in gearboxes [2]. Some of the excitations are caused by manufacturing-related deviations $w(t)$, such as gear manufacturing errors, profile errors or shaft misalignments. Under load, a major excitation mechanism is the non-constant mesh stiffness $c_s(t)$. The mesh stiffness varies during the rotation because there are not always the same number of teeth in mesh

and because the stiffness of a single tooth $c_i(t)$ depends also on its position. Mathematically, this parametric oscillation can be described with the gear model in Figure 1 and the equations given in (1) (2). The equations can be further simplified to a single spring-mass system (6) [1].

$$J_1\ddot{\phi}_1 = -c_s(t)r_1(r_1\phi_1 - r_2\phi_2 - w(t)) - dr_1(r_1\dot{\phi}_1 - r_2\dot{\phi}_2 - \dot{w}(t)) + M_1 \quad (1)$$

$$J_2\ddot{\phi}_2 = c_s(t)r_2(r_1\phi_1 - r_2\phi_2 - w(t)) + dr_2(r_1\dot{\phi}_1 - r_2\dot{\phi}_2 - \dot{w}(t)) + M_2 \quad (2)$$

$$x = r_1\phi_1 - r_2\phi_2 - w(t) \quad (3) \quad M = \frac{M_1r_1}{J_1} - \frac{M_2r_2}{J_2} \quad (4) \quad \frac{1}{m} = \frac{r_1^2}{J_1} + \frac{r_2^2}{J_2} \quad (5)$$

$$\ddot{x} + \frac{d}{m}\dot{x} + \frac{c_s(t)}{m}x + \ddot{w}(t) = M \quad (6)$$

Methods for noise and vibration reduction

In addition to a high manufacturing quality, noise reduction methods can be divided into constructive, passive and active methods. Constructive methods try to achieve a low variation in the gear stiffness $c_s(t)$ by changing the tooth design. Passive methods use damping materials to reduce the transmission of vibration and sound. Active vibration control (AVC) systems measure the vibrations with an accelerometer and try to generate a vibration with the same amplitude and opposite phase that is superimposed on the undesired vibration. This theoretically cancels the vibration and the resulting noise. AVC methods differ in the number, placement, and choice of actuator used to generate the compensating vibration (Figure 2).

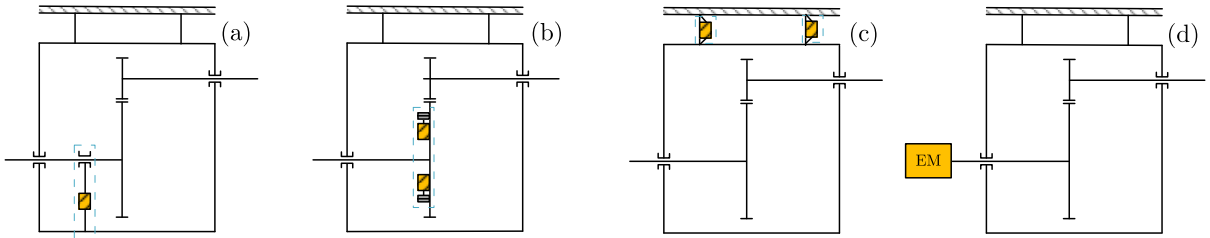


Fig. 2: Overview of methods for active vibration control of gearboxes [3]

Concept (a) presented by Montague et. al. [4] is the first research in which active vibration control has been applied to transmissions. A piezoelectric actuator was used which transmits a compensation force to the shaft via an additional bearing. At a gear meshing frequency of 4500 Hz, vibrations could be damped by 70%. Chen and Brennan [5] suggested a control system in which three inertial mass actuators mounted directly on the gear generate centrifugal forces to suppress vibrations (b). Experimental results showed a reduction of about 7 dB in acceleration at gear meshing frequencies between 150 Hz and 350 Hz. Concepts based on figure (c) employ active controlled struts to minimize vibrations in the recording structure [6]. The concept (d) published by Benzel [7] [8] achieves noise reduction by a harmonic motor torque M_c . The idea is based on converting the parameter oscillation from Equation (6) into a forced harmonic oscillation (7) and the compensation of the applied force term with M_c .

$$\ddot{x} + \frac{d}{m}\dot{x} + \frac{c_{s,0} + \sum_{n=1}^N c_{s,i} \sin(n\omega t + \varphi_n)}{m}x = M \Rightarrow \ddot{x} + \frac{d}{m}\dot{x} + \frac{c_{s,0}}{m}x = M - \frac{\sum_{n=1}^N c_{s,i} \sin(n\omega t + \varphi_n)}{m} + M_c \quad (7)$$

Experimental studies on a drive train with a power of 0.8 kW and a two-stage gearbox show a reduction in acceleration of 14 dB. One advantage of this concept is that no additional actuator is required. A disadvantage is that an experimental analysis is required in advance of how the drive torque affects the error signal, known as secondary path identification. An inaccurate identification of the secondary path, or a change during operation, can cause the algorithm to become unstable. The limited bandwidth of the current controller can furthermore exclude the application range for high frequencies. Therefore,

this paper presents a method to determine the required compensation torque online and without prior experimental analysis of the secondary path. In addition, a control structure for controlling the high-frequency currents is presented.

Narrowband active vibration control

The basic configuration of the drive system consists of a spur gear, a permanent-magnet synchronous machine and an inverter (Figure 3). The current control is designed as a field-oriented control and the rotor position is measured with an incremental encoder. For active vibration control, an accelerometer is attached to the gearbox to measure the vibrations. The AVC algorithm controls the phase and amplitude of the required compensation torque respectively the compensation current. The current is then set by a controller located in parallel with the dq current control.

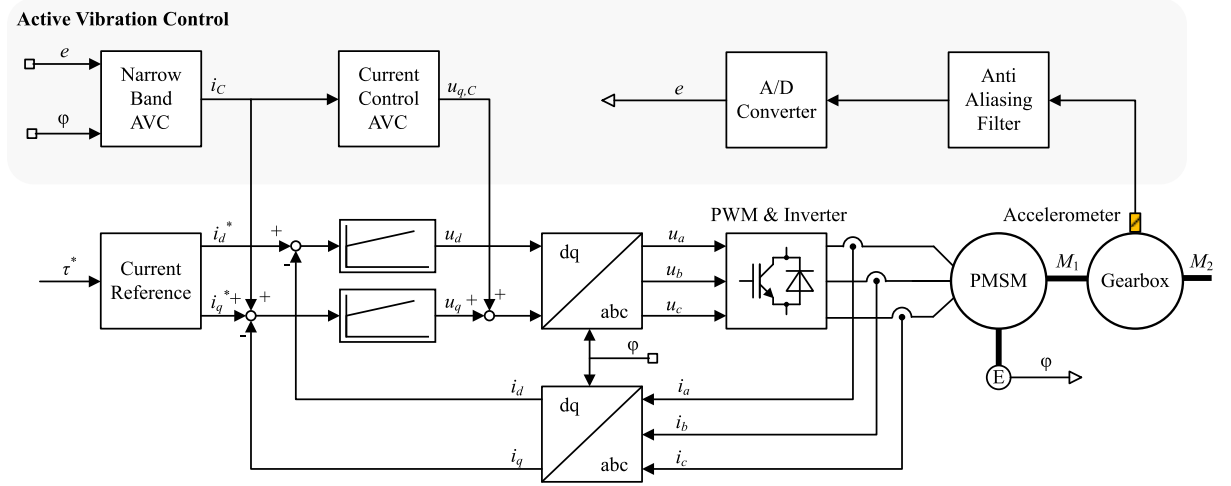


Fig. 3: Fundamental structure of the control system

The active vibration control is a narrowband implementation as shown in Figure 4. Narrowband AVC algorithms offer the advantage that individual frequency components can be selectively damped [9]. The individual frequency components operate in parallel. The system controls the required output signal by adaptive filtering of a periodic reference signal. The reference signal can be generated synthetically or measured by a measurement system. Since the gear mesh vibrations are multiples of the mechanical rotor frequency, the measured rotor position is used as the reference signal. To determine the frequency component of the gear meshing frequency, the rotor position is multiplied by the number of teeth of the pinion and the respective harmonic z_n . A sine and cosine component is formed from the reference signal, and the amplitude and phase of the output signal are adjusted by adjusting the weights of the adaptive filter (see equation (8),(9)). The transfer function $S(z)$ describes the secondary path, which is the path between the output of the adaptive filter and the input of the error sensor. In this application, the secondary path consists of the transfer behavior of the current controller, the PWM, the inverter, the electric machine, the gearbox, the accelerometer and the anti-aliasing filter.

$$\underline{w} = w_a + i w_b \quad (8) \quad \underline{i}_{C,n}(k) = \underline{w} \cdot e^{iz_n\varphi(k)} \quad (9) \quad \underline{E} = e_{a,n} + ie_{b,n} \quad (10)$$

$$\underline{e}_n(k) = \underline{E} \cdot e^{iz_n\varphi(k)} = \underline{P} \cdot e^{iz_n\varphi(k)} + \underline{S} \cdot \underline{w} \cdot e^{iz_n\varphi(k)} \quad (11)$$

The weights are adjusted by the simultaneous equation method [10]. The basic idea of this method is to measure the output behavior of the filter weights and to calculate the new filter weights based on the change in the error signal. Compared to other methods such as the FxLMS algorithm [11], no accurate model of the secondary path is required. The simultaneous equation algorithm works blockwise. The initial weights of the algorithm are adjusted only every N time steps and are kept constant during that time. The algorithm assumes that the complex error signal of the past time period \underline{E}_0 , the current time

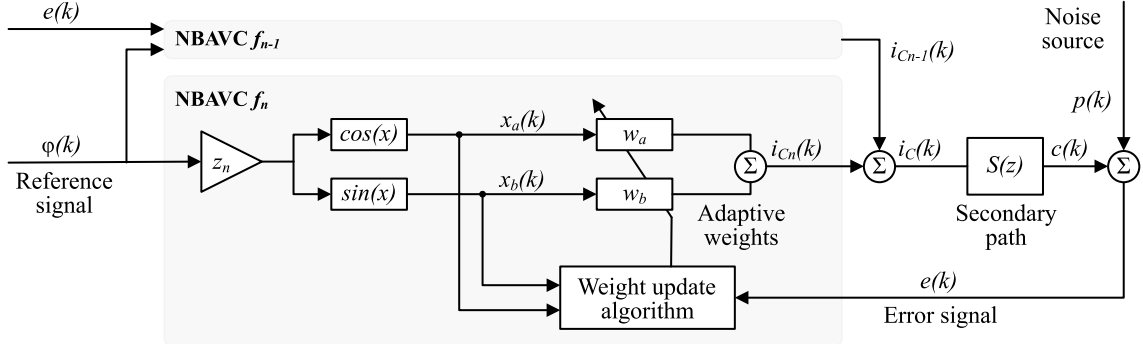


Fig. 4: Narrow band active vibration control

period E_1 and the future time period E_2 for one frequency component can be described with the following equations.

$$E_0 = P_0 + \underline{S} \cdot \underline{w}_0 \quad (12) \qquad E_1 = P_1 + \underline{S} \cdot \underline{w}_1 \quad (13) \qquad 0 = P_2 + \underline{S} \cdot \underline{w}_{opt} \quad (14)$$

This system of equations can be used to determine the optimal weights w_{opt} :

$$\underline{w}_{opt} = \frac{E_0 \cdot \underline{w}_1 - E_1 \cdot \underline{w}_0}{E_0 - E_1} \quad (15)$$

Since the error signal consists of several frequencies, the complex Fourier coefficients for the frequency component must be calculated.

$$e_{a,n} = \frac{1}{N} \sum_{k=0}^{N-1} e(k) \cdot \cos\left(\frac{2\pi z_n k}{N}\right) = \frac{1}{N} \sum_{k=0}^{N-1} e(k) \cdot \cos(z_n \varphi(k)) = \frac{1}{N} \sum_{k=0}^{N-1} e(k) \cdot x_a(k) \quad (16)$$

$$e_{b,n} = \frac{1}{N} \sum_{k=0}^{N-1} e(k) \cdot \sin\left(\frac{2\pi z_n k}{N}\right) = \frac{1}{N} \sum_{k=0}^{N-1} e(k) \cdot \sin(z_n \varphi(k)) = \frac{1}{N} \sum_{k=0}^{N-1} e(k) \cdot x_b(k) \quad (17)$$

An abrupt change of the filter weights excites the mechanical system to oscillate. In addition, the error signal is provided with measurement uncertainties. For these reasons, the update of the filter weights is done stepwise (18). At a step size of $\mu = 1$, the algorithm converges fast. Smaller step sizes result in slower but more stable convergence behavior.

$$\underline{w}_2 = (1 - \mu) \cdot \underline{w}_1 + \mu \cdot \underline{w}_{opt} \quad (18)$$

Control of the harmonic currents

In addition to determining the required filter weights and the required compensation current, the current must also be controlled for higher frequencies. The existing dq current control might not have the required bandwidth. Also, the compensation current can be in the range of the measurement noise of the current sensor. For these reasons, compensation current control is implemented as feedforward control in parallel with the dq current control (Figure 3). The control is performed by a PDT1 controller (Figure 5) whose output signal is added to the q-component of the desired voltage.

The feedforward controller (equation 19) is parameterized so that the numerator polynomial of the controller compensates the denominator polynomial of the controlled system (equation 20). For this ap-

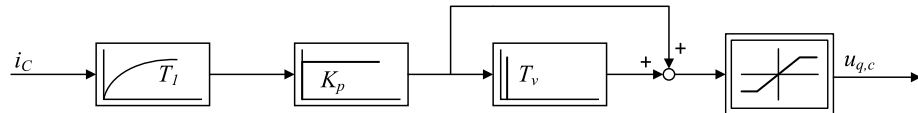


Fig. 5: Current controller for active vibration control

plication case of a permanent-magnet synchronous machine controlled via a field-oriented control, T_s describes the time constant of the motor winding. The derivative time T_v of the differentiator is set to the time constant T_s . T_σ is the equivalent time constant of the actuator, in this case the inverter including the PWM. The parameter T_1 can be used to set the cut-off frequency and thus the usable range of the control. The parameter T_1 was set equal to the time constant T_σ . In addition, the output of the feedforward control was limited.

$$G_s = \frac{K_s}{1 + s \cdot T_s} \cdot \frac{1}{1 + s \cdot T_\sigma} \quad (19)$$

$$G_c = K_p \cdot \frac{1 + s \cdot T_v}{1 + s \cdot T_1} \quad (20)$$

$$K_p = \frac{1}{K_s} = R_s \quad (21)$$

$$T_v = T_s = \frac{L_q}{R_s} \quad (22)$$

$$T_\sigma \leq T_1 \leq T_s \quad (23)$$

Test bench and experimental results

The experimental tests were carried out on the test bench shown in Figure 6. The drive train consists of a three-stage spur gear and a two-stage planetary gear (3), which are connected via a differential. The planetary gear is driven by an induction machine (2) with a power of 60kW. A permanent magnet synchronous machine (PMSM) (1) with a rated power of 75kW is mounted on the spur gear. Both electrical machines are powered by a three-phase inverter with a switching frequency of 36kHz. Active vibration control was tested on the first stage, the high speed stage, of the spur gearbox. The PMSM is used as actuator. The first gear stage consists of helical gearing with a ratio of $i = 4$. The pinion has 19 teeth, resulting in a gear mesh frequency of $f_{z1} = \frac{19 \cdot n}{60}$ for the first harmonic and $f_{z2} = \frac{38 \cdot n}{60}$ for the second harmonic.

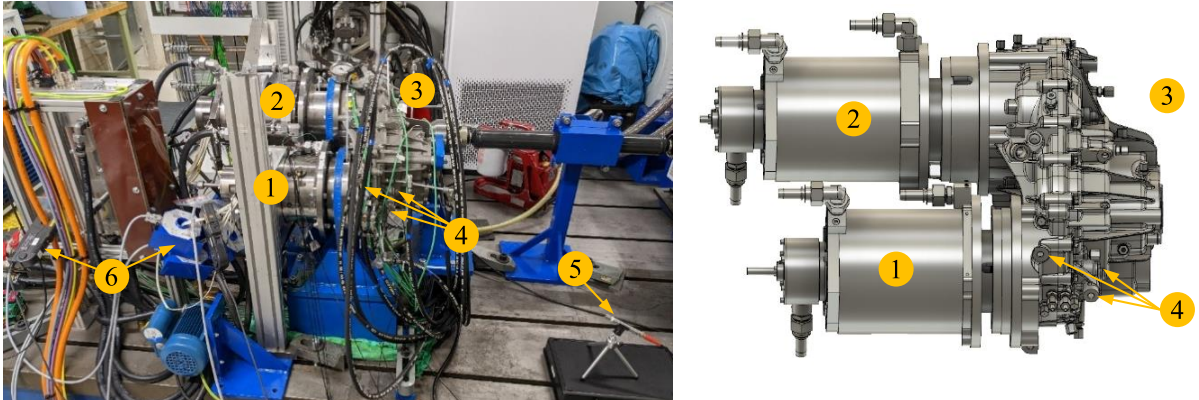


Fig. 6: Test bench for experimental evaluation

Measurement sensors are 4 accelerometers (4) mounted on the gearbox and a microphone (5) as well as a measurement of the DC and AC current of the inverter (6). The accelerometer for the control is mounted directly on the bearing of the first stage and measures the radial acceleration. Besides there is another accelerometer (sensor 1) which is used for evaluation. Another accelerometer (sensor 2) measures the axial movement of the gearbox and is also located near the bearing. Sensor 3 is mounted on the gearbox housing near the permanent magnet synchronous machine. The microphone is placed at a distance of approximately 1 m from the drive train.

The results for the steady-state operating point with the speed of $n = 7000\text{min}^{-1}$ and a load of $M = 15\text{Nm}$ are shown in Fig. 7. Shown are the accelerations of sensors 1 and 2 and the sound pressure level of the microphone. The blue line is the signal without active vibration control. In orange is drawn the spectrum of the algorithm using the simultaneous equation method. The algorithm updates its output weights for the first gear mesh frequency every 5 rotations and calculates the fourier analysis of the error signal over the same period. The value of the step size μ is 0.1. For comparison, the results of the filtered-x-LMS (FxLMS) algorithm were also shown. For the FxLMS algorithm, the secondary path was determined

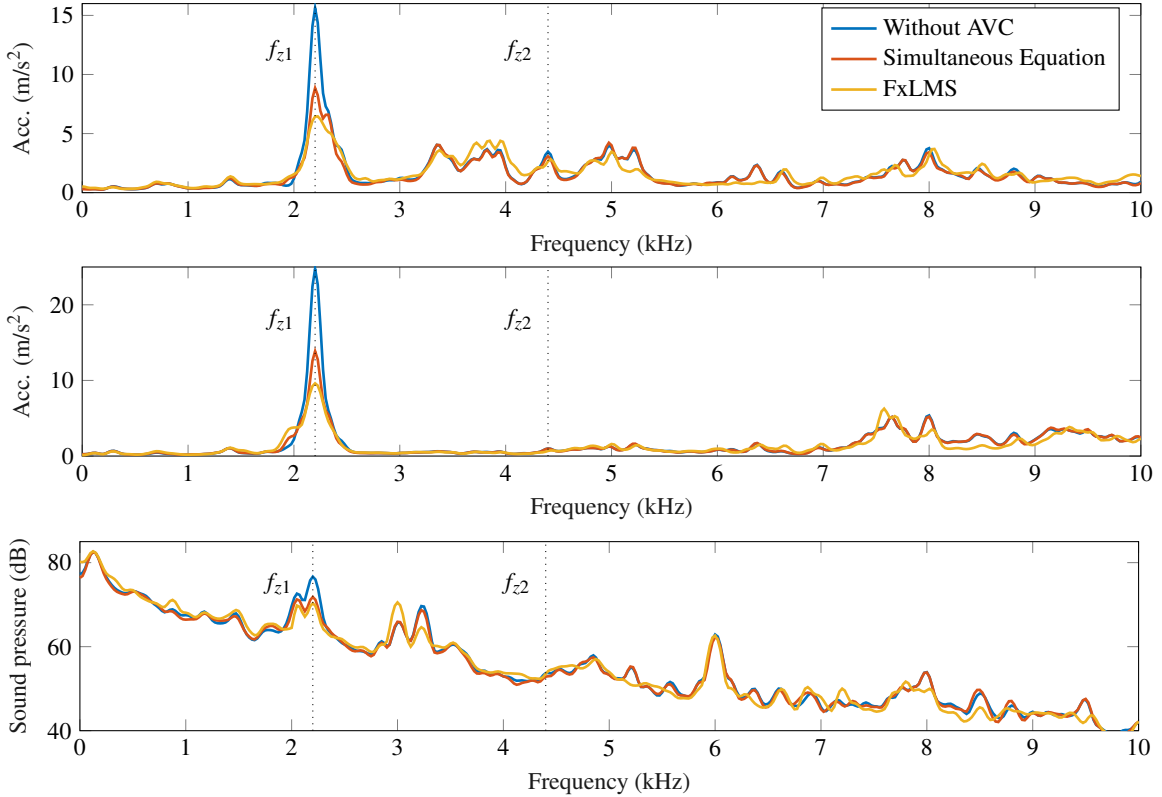


Fig. 7: Operating point 7000min^{-1} 15Nm; sensor 1 (top), sensor 2 (middle), microphone (bottom)

using a random noise signal. The step size μ is also set to 0.1, and the algorithm updates its output weights at a frequency of 100Hz.

When comparing the signals, it can be seen that both methods can reduce the vibrations in radial and axial direction. With the microphone, a reduction in noise of about 5 dB can also be measured for the first gear mesh frequency. The second gear mesh frequency causes only minor radial forces and is negligible for this operating point. The frequency spectrum also shows further acceleration components, which can be assigned to the other gear stages and the electrical machines. Furthermore, it can be seen that the vibrations are damped slightly better with the FxLMS algorithm. With both algorithms, the amplitude of the compensation current I_c is limited to 25A, which is about 10% of the rated current. By increasing this limit, the vibrations can be further damped.

The power consumption measured at the input of the inverter is 11.27kW without compensation and 11.68kW with compensation (SE method). In the DC and AC current of the inverter, the components of the active vibration control are clearly noticeable (Figure 8).

Table I shows the acceleration of the first mesh frequency for other operating points. The acceleration with compensation here refers to the simultaneous equation method. When comparing the operating

Speed	Torque	Sensor 1		Sensor 2		Sensor 3		Microphone	
		Without	With	Without	With	Without	With	Without	With
5000min^{-1}	5Nm	3.6m/s ²	1.8m/s ²	3.2m/s ²	0.9m/s ²	0.4m/s ²	0.4m/s ²	70dB	68dB
5000min^{-1}	15Nm	2.7m/s ²	1.4m/s ²	3.3m/s ²	1.6m/s ²	0.4m/s ²	0.4m/s ²	70dB	68dB
7000min^{-1}	5Nm	15m/s ²	9.1m/s ²	20m/s ²	13m/s ²	4.2m/s ²	2.7m/s ²	74dB	70dB
7000min^{-1}	15Nm	15m/s ²	8.7m/s ²	24m/s ²	14m/s ²	7.0m/s ²	4.1m/s ²	77dB	72dB

Table I: Accelerations without and with active noise control

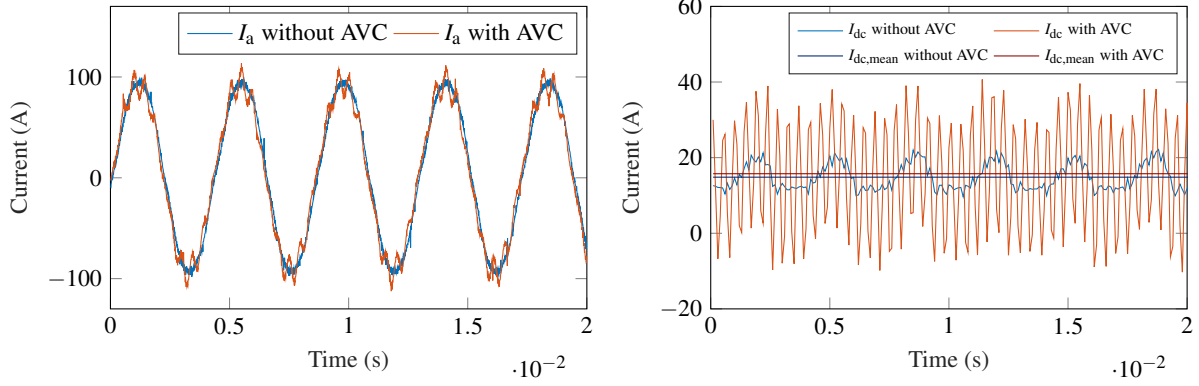


Fig. 8: Measured currents of the inverter, alternating current (left) and direct current (right)

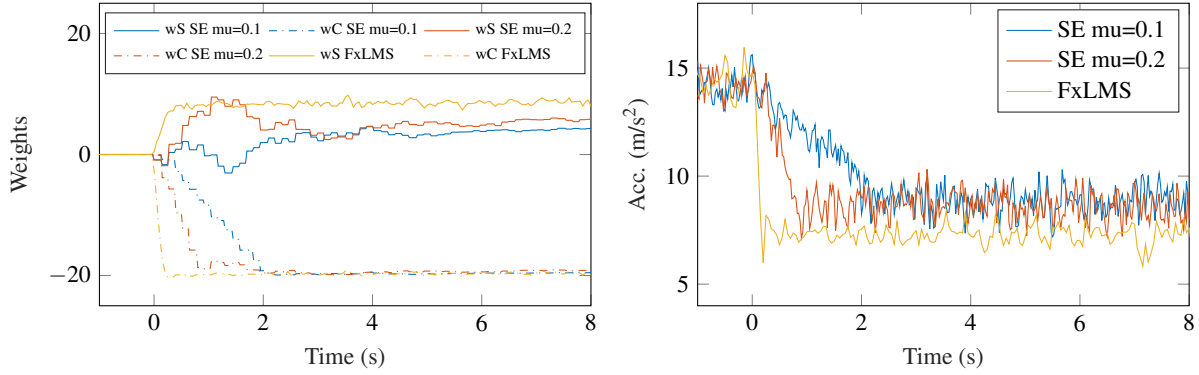


Fig. 9: Evolution of filter weights (left) and acceleration at first mesh frequency (right)

points, it can be seen that the acceleration increases from 5000min^{-1} to 7000min^{-1} . The achievable vibration and noise reduction is greater for the 7000min^{-1} speed.

The convergence behavior of the algorithm for the steady-state operating point at a speed of 7000min^{-1} and a torque of $M = 15\text{Nm}$ is shown in Figure 9. The left figure shows the two output weights and the right figure shows the amplitude of the acceleration of the first mesh frequency $|E_{fz1}|$. The algorithm is activated at time $t = 0$. Increasing the step size μ from 0.1 to 0.2 results in faster convergence. The variance of the output weights for the steady state value is similar for these two step sizes. The FxLMS algorithm converges even faster due to its higher update rate. It also achieves a slightly different final value for the sinusoidal output weight and achieves a slightly better reduction.

Figure 10 shows the behavior of the algorithm with a change in speed. On the left side are again the filter

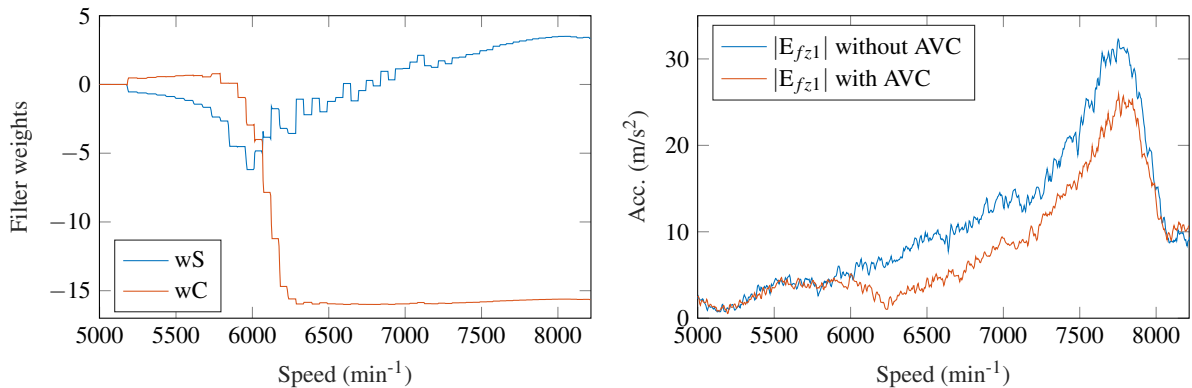


Fig. 10: Behavior under speed change: filter weights (left) and acceleration (right)

weights and on the right side the acceleration of the first gear mesh frequency. The algorithm is activated at a speed of 5200min^{-1} and then also converges to the values in Figure 9. As the filter weights reach this value, a reduction in acceleration is measurable. The acceleration increases up to a speed of 7700min^{-1} and then decreases again. At this speed or excitation frequency, there is a resonance of the mechanical structure. In general, it can be seen that the algorithm remains stable despite changes in speed. The reduction remains the same over the speed range.

Conclusion

The non-constant gear stiffness generates torque pulsations during power transmission in gearboxes. This leads to unwanted vibrations and noise. An approach was presented that reduces the torque pulsations with the electric machine and actively damps the resulting vibrations and noise. For this purpose, a method was investigated with which the amplitude and the phase of the compensation current can be calculated without a model of the secondary path. In addition, a control structure was presented with which the high-frequency current can be controlled. Experimental tests of the method show that active damping of vibration and noise is possible. A comparison with the simultaneous equation method versus the FxLMS algorithm shows that the FxLMS algorithm achieves a slightly better reduction. If a determination of the secondary path is not possible, the simultaneous equation method can be used. In the other case the use of the FxLMS algorithm is preferable.

References

- [1] Sanzenbacher S.: Reduction of transmission noises by mitigation of structure-borne sound, Stuttgart: Institut für Maschinenelemente, 2016, ISBN 978-3-936100-66-2
- [2] Smith J. D.: Gear noise and vibration, CRC press, 2nd edition, 2013, ISBN 978-0824741297
- [3] Zech, P.: Aktive Reduktion modulierter Zahneingriffsvibrationen von Planetengetrieben. *Shaker Verlag*, 2019
- [4] Montague, G. T., Kascak, A. F., Palazzolo, A., Manchala, D.: Feedforward control of gear mesh vibration using piezoelectric actuators. *Shock and Vibration*, vol. 1, no. 5, pp. 473-484, 1994
- [5] Chen, M. H., Brennan, M. J.: Active control of gear vibration using specially configured sensors and actuators. *Smart Materials and Structures*, vol. 9, no. 3, pp. 342, 2000
- [6] Sutton, T. J., Elliott, S. J., Brennan, M. J., Heron, K. H., Jessop, D. A. C.: Active isolation of multiple structural waves on a helicopter gearbox support strut. *Journal of Sound and Vibration*, vol. 205, no. 1, pp. 81-101, 1997
- [7] Benzel, T., Möckel, H. A.: Active control of gear pair vibration with an electronically commutated motor as actuator. In *4th International Electric Drives Production Conference (EDPC)*, pp. 1-6, IEEE, 2014
- [8] Benzel, T., Möckel, H. A.: Active gear pair vibration control during non-static load and speed with an electronically commutated motor as actuator. In *10. ETG/GMM-Symposium Innovative small Drives and Micro-Motor Systems (IKMT)*, pp. 1-6, VDE, 2015
- [9] Kuo, S. M., Morgan, D. R.: Active noise control: a tutorial review. *Proceedings of the IEEE*, 87.6, pp. 943-973, 1999
- [10] Zech, P., Plöger, D. F., Rinderknecht, S.: Active control of planetary gearbox vibration using phase-exact and narrowband simultaneous equations adaptation without explicitly identified secondary path models. *Mechanical Systems and Signal Processing*, vol. 120, pp. 234-251, 2019
- [11] Burgess, John C.: Active adaptive sound control in a duct: A computer simulation. *The Journal of the Acoustical Society of America*, vol. 70, no. 3, pp. 715-726, 1981